NASA Technical Memorandum 104143

UNSTRUCTURED-GRID METHODS DEVELOPMENT FOR UNSTEADY AERODYNAMIC AND AEROELASTIC ANALYSES

JOHN T. BATINA
ELIZABETH M. LEE
WILLIAM L. KLEB
RUSS D. RAUSCH

SEPTEMBER 1991

National Aeronautics and Space Administration

Langley Research Center
Hampton, Virginia 23665

UNSTRUCTURED-GRID METHODS DEVELOPMENT FOR UNSTEADY AERODYNAMIC AND AEROELASTIC ANALYSES

John T. Batina
Elizabeth M. Lee
William L. Kleb
NASA Langley Research Center
Hampton, Virginia 23665–5225 USA

and

Russ D. Rausch
Purdue University
West Lafayette, Indiana 47907 USA

Summary

The current status of unstructured-grid methods development in the Unsteady Aerodynamics Branch at NASA Langley Research Center is described. These methods are being developed for unsteady aerodynamic and aeroelastic analyses. The paper first highlights the flow solvers that have been developed for the solution of the unsteady Euler equations and then gives selected results which demonstrate various features of the capability. The results demonstrate two- and three-dimensional applications for both steady and unsteady flows. Comparisons are also made with solutions obtained using a structured grid code and with experimental data to determine the accuracy of the unstructured grid methodology. These comparisons show good agreement which thus verifies the accuracy.

Introduction

Considerable progress has been made over the past two decades on developing computational fluid dynamics (CFD) methods for aerodynamic analysis.[1,2] Recent work in CFD has focused primarily on developing algorithms for the solution of the Euler and Navier-Stokes equations. For unsteady aerodynamic and aeroelastic analysis, these methods generally require that the mesh move to conform to the instantaneous position of the moving or deforming body under consideration. Many of the methods that are currently being developed assume that the mesh moves rigidly or that the mesh shears as the body deforms. These assumptions consequently limit the applicability of the procedures to rigid-body motions or small-amplitude deformations. Furthermore, these methods of solution typically assume that the computational grid has an underlying geometrical structure. As an alternative, algorithms have been developed recently which make use of unstructured grids.[3–19] In two dimensions these grids are typically made up of triangles and in three dimensions they consist of an assemblage of tetrahedra.

The unstructured grid methods have several distinct advantages over structured grid methods which make them attractive for unsteady aerodynamic and aeroelastic analyses. For example, the primary advantage of the unstructured grid methodology is the ability to easily model very complicated three-dimensional geometries such as the F/A-18 aircraft shown in Fig. 1.[9] The aircraft was modeled by including the wings with leading edge extension, horizontal and vertical tails, as well as the canopy and the fuselage. The modeling also includes engine inlets and nozzles to simulate engine power effects. With a structured grid, it is extremely difficult to achieve this level of geometrical complexity. A second advantage is that the methodology allows for a general way to move the mesh to treat realistic motions and structural deformations of complete aircraft configurations. An example of the deforming surface grid for a transport-type configuration undergoing a complete-vehicle bending motion is depicted in Fig. 2. The deforming grid capability does not involve any assumptions which limit applications to small deformations, such as the simple grid shearings done in some structured grid codes. A third advantage is that it enables in a natural way for adaptive mesh refinement to predict more accurately the physics for the flow. For example, shown in Fig. 3 is a conical vortex-dominated flow solution for a flat plate delta wing at a supersonic freestream Mach number.[13] The solution was obtained by adapting the original coarse mesh three times to the instantaneous flow. The final result is a highly accurate solution of the Euler equations, produced by using an order of magnitude fewer grid points than if a globally fine mesh was used. Similar to spatial adaption, temporal adaption may also be employed with unstructured grids for unsteady problems to resolve more accurately and efficiently the physics of the flow in time.[18] Temporal adaption can be thought of as time-accurate local time-stepping where smaller time steps are used in grid cells where the temporal gradients are large and larger time steps are used in cells where the gradients are small. Time accuracy is maintained by bringing all grid cells to the same time level as determined by the largest step size in the problem.

The purpose of the paper is to describe the current status of unstructured-grid methods development within the Unsteady Aerodynamics Branch at NASA Langley Research Center.[10–19] The paper first highlights the flow solvers that have been developed for solution of the time-dependent Euler equations and then gives selected results which demonstrate various features of the capability. The flow solvers that are described are either of the central-difference-type with explicit artificial dissipation or of the upwind-type which are naturally dissipative. Both implicit and explicit temporal discretizations are discussed for the time-integration of the governing fluid flow equations. Details on the spatial and temporal adaption procedures are also

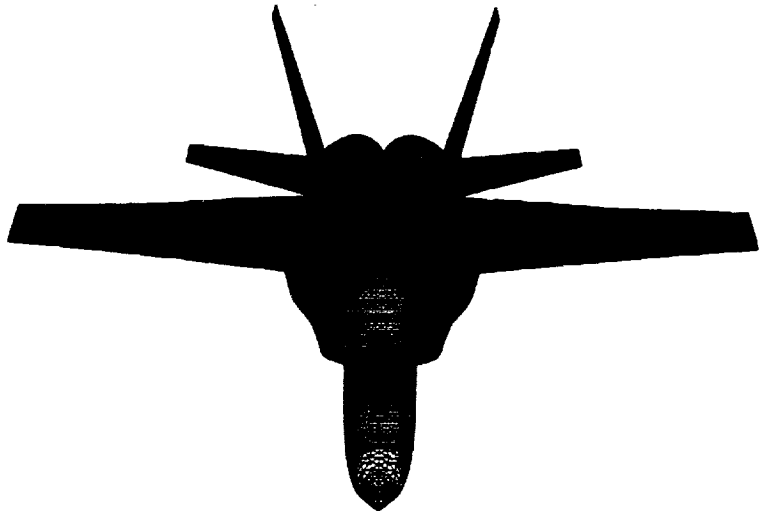

Fig. 1 Unstructured surface grid for F/A 18 fighter configuration.

given. The selected results that are presented demonstrate two- and three-dimensional applications for both steady and unsteady flows. Comparisons are also made with solutions obtained using a structured grid code and with experimental data to determine the accuracy of the unstructured grid methodology.

Central-Difference-Type Flow Solver

The unsteady Euler equations in integral form are solved using a finite-volume algorithm that was developed for use on unstructured grids of triangles in 2D or tetrahedra in 3D.[10-14] The algorithm reduces conceptually to central differencing on a rectangular mesh and thus is referred to as a central-difference-type flow solver. With this solver, artificial dissipation is added explicitly to prevent oscillations near shock waves and to damp high-frequency uncoupled error modes. Specifically, an adaptive blend of harmonic and biharmonic operators is used, corresponding to second and fourth difference dissipation, respectively. The biharmonic operator provides a background dissipation to damp high frequency errors and the harmonic operator prevents oscillations near shock waves.

The Euler equations are integrated in time using a standard, explicit, four-stage, Runge-Kutta time-stepping scheme. In this scheme the convective operator is evaluated at each stage and, for computational efficiency, the dissipative operator is evaluated only at the first stage. The scheme is second-order-accurate in time and includes the necessary terms to account for changes in cell volumes due to a moving or deforming mesh. Furthermore, this explicit-scheme has a step size that is limited by the Courant-Friedricks-Lewy (CFL) condition corresponding to a CFL number of $2\sqrt{2}$. To accelerate convergence to steady-state, the CFL number may be increased by averaging implicitly the residual with values at neighboring grid points. These implicit equations are solved approximately using several Jacobi iterations. Convergence to steady-state is further accelerated using enthalpy damping and local time stepping. The local time stepping uses the maximum allowable step size at each grid point as determined by a local stability analysis. For unsteady applications, however, a global time step is usually used because of the time-accuracy requirement. The maximum allowable global time step may be increased to a value that is larger than that dictated by the CFL condition by using a time accurate version of the residual smoothing. Alternatively, temporal adaption may be used which involves a spatially varying time step, as described in a subsequent section.

Upwind-Type Flow Solver

The unsteady Euler equations may be solved alternatively by using upwind differencing and either flux-vector or flux-difference splitting similar to upwind schemes developed for use on structured meshes.[10, 15-19] The present unstructured grid algorithm is thus referred to as an upwind-type flow solver. The spatial discretization of this solver involves a so-called flux-split approach based on either the flux-vector splitting of van Leer[20] or the flux-difference splitting of Roe.[21] These flux-split discretizations account for the local wave-propagation characteristics of the flow and they capture shock waves sharply with at most one grid point within the shock structure. A further advantage is that these discretizations are naturally dissipative and consequently do not require additional artificial dissipation terms or the adjustment of free parameters to control the dissipation.

The Euler equations are integrated in time using either an explicit Runge-Kutta method (described in the previous section) or an implicit time-integration scheme involving a Gauss-Seidel relaxation procedure.[15] The procedure is implemented by reordering the elements that make up the unstructured mesh from upstream to downstream. The solution is obtained by sweeping two times through the mesh as dictated by stability considerations. The first sweep is performed in the direction from upstream to downstream and the second sweep is from downstream to upstream. For purely supersonic flows the second sweep is unnecessary. This relaxation scheme is unconditionally stable and thus allows the selection of the step size based on temporal accuracy of the problem being considered, rather than on the numerical stability of the algorithm. Consequently, very large time steps may be used for rapid convergence to steady state, and an appropriate step size may be selected for unsteady cases, independent of numerical stability issues.

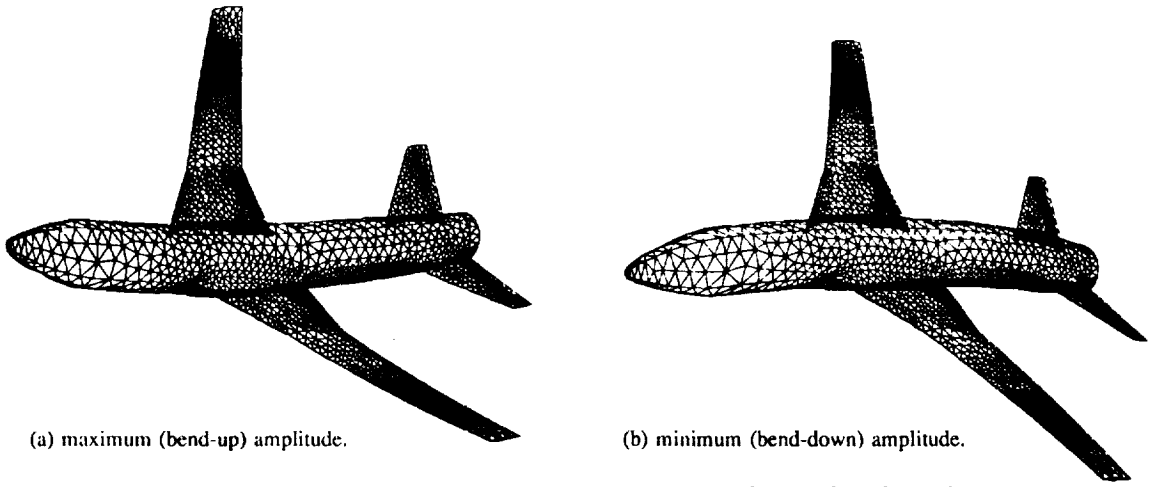

(a) maximum (bend-up) amplitude.

(b) minimum (bend-down) amplitude.

Fig. 2 Surface grid for the Pathfinder I configuration which illustrates how the mesh moves for an assumed complete-vehicle bending mode.

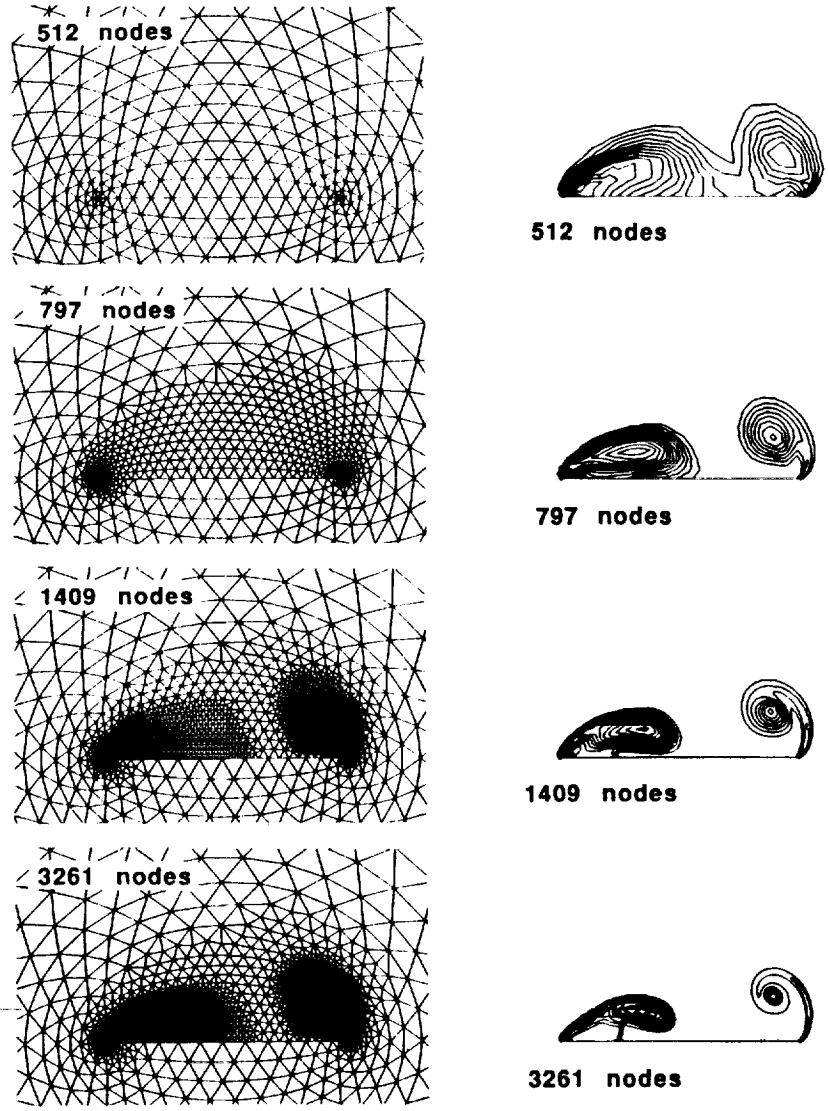

Fig. 3 Effects of adaptive mesh refinement on the total pressure loss contours for a 75° swept flat-plate delta wing computed using the conical Euler equations at $M_\infty = 1.4$, $\alpha = 20°$, and $\beta = 10°$.

Spatial Adaption Procedure

Spatial adaption is employed with the unstructured grid flow solvers to enrich the mesh locally in regions of high spatial flow gradients to resolve more accurately and efficiently the physics of the flow.[13] Equally attractive are coarsening techniques that remove elements from regions where relatively small changes in the flow variables occur. Both enrichment and coarsening procedures are currently being developed.[19] However, only the enrichment procedure is described herein. The enrichment procedure uses an indicator to determine if an element in the mesh is to be refined or subdivided into smaller elements. Typically, the absolute change in density along an edge is used as an indicator for flows with shock waves and total pressure loss is used for flows with vortices. More recently a refinement indicator based on the material derivative of density[19] has been shown to be a superior indicator for unsteady flows. In general, the refinement indicator is compared with a preset tolerance to determine whether a given element should be refined. If the tolerance is exceeded, a new node is created at the midpoint of the edge and the element is divided. Each time the mesh is refined, an element may be divided in one of several different ways. The coordinates of the new node are determined by averaging the coordinates of the endpoints that make up the bisected edge. Special care must be taken, however, when an edge that is to be divided lies on a boundary of the grid, since the midpoint of the edge does not generally lie on the boundary. In this case, the location of the new node is determined generally by using a spline of the boundary coordinates.

Temporal Adaption Procedure

Temporal adaption is employed with the unstructured grid flow solvers, similar to spatial adaption, to resolve more accurately and efficiently the physics of the flow in time.[18] Temporal adaption can be thought of as time-accurate local time-stepping. Local time-stepping is typically used in a non-time-accurate manner to accelerate the convergence of the governing fluid flow equations to steady-state. Since only steady-state is desired, it does not matter that every point in the flow is at a different time. This, of course, is not the case for a time-accurate problem, since each point in the flow for such a calculation must be on the same temporal level to maintain time-accuracy. The problem is that if all of the grid cells are marched at the same time step with an explicit time-marching scheme, the most restrictive time step must be used in order to maintain numerical stability. Temporal adaption is a method to march each cell at its own time step, although ultimately the flow variables in all cells reach the same point in time. Temporal adaption can be viewed as similar to spatial adaption in that small time steps should be taken only in localized areas governed by the flow physics and not in the entire flow field. Typically, small grid cells are integrated with small time steps and large grid cells are integrated with large time steps. All of the cells reach the same time level $n + 1$ to maintain time-accuracy by using local time steps that are multiples of one another. The solution is integrated in a special sequence so that all values necessary for the calculations at an intermediate level are available at the proper times. For a particular cell to be integrated from time level n to time level $n + 1$, for example, the solution must also be known at its neighboring cells at time level n. If the value needed for the integration is unknown at a particular temporal node, it is determined from a linear interpolation between two known values.

Deforming Mesh Algorithm

For problems where the aircraft moves or deforms, the mesh must move so that it continuously conforms to the instantaneous shape or position of the vehicle. This is accomplished by using a spring network to model the original mesh such that each edge of the triangle or tetrahedron is represented by a spring.[12] The spring stiffness for a given edge is taken to be inversely proportional to the length of the edge. Grid points on the outer boundary of the mesh are held fixed and the instantaneous locations of the points on the inner boundary (aircraft) are given by the prescribed surface motion. At each time step, the static equilibrium equations in the x, y, and z directions, which result from a summation of forces, are solved iteratively at each interior node of the grid for the displacements. This is accomplished by using a predictor-corrector procedure, which first predicts the displacements of the nodes by extrapolation from grids at previous time levels and then corrects these displacements using several Jacobi iterations of the static equilibrium equations. The predictor-corrector procedure has been found to be more efficient than simply performing Jacobi iterations because far fewer iterations are required to achieve acceptable convergence. In practice it has been found that only one or two iterations are sufficient to accurately move the mesh.

Results and Discussion

Selected results from the unstructured-grid methods of Refs. 10-19 are presented for two- and three-dimensional geometries for both steady and unsteady flows. Comparisons are made with solutions obtained using a structured grid code and with experimental data to determine the accuracy of the methodology.

Two-Dimensional Euler Results

To assess the two-dimensional central-difference-type Euler flow solver, calculations were performed for the NACA 0012 airfoil.[11] These results were obtained using the unstructured grid shown in Fig. 4. The grid has 3300 nodes, 6466 triangles, and extends 20 chordlengths from the airfoil with a circular outer boundary. Also there are 110 points that lie on the airfoil surface. Generalized aerodynamic forces for the NACA 0012 airfoil oscillating in either plunge or pitch-about-the quarter-chord

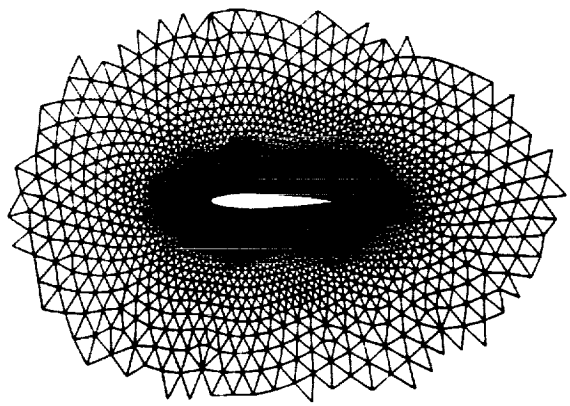

Fig. 4 Partial view of unstructured grid of triangles about the NACA 0012 airfoil.

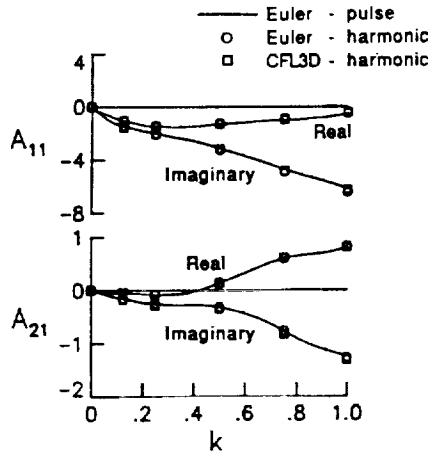

(a) due to plunge.

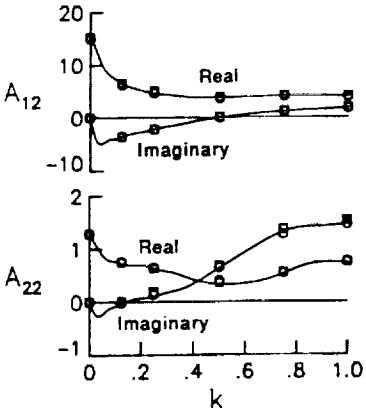

(b) due to pitch.

Fig. 5 Comparisons of generalized aerodynamic forces computed using CFL3D and the unstructured-grid central-difference-type Euler flow solver for the NACA 0012 airfoil at M_∞ = 0.8 and α_o = 0°.

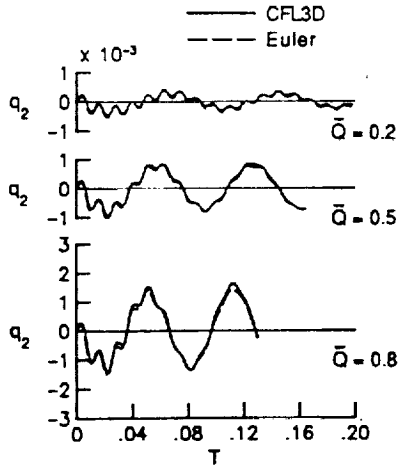

Fig. 6 Comparisons of generalized displacements computed using CFL3D and the unstructured-grid central-difference-type Euler flow solver for the NACA 0012 airfoil at M_∞ = 0.8 and α_o = 0°.

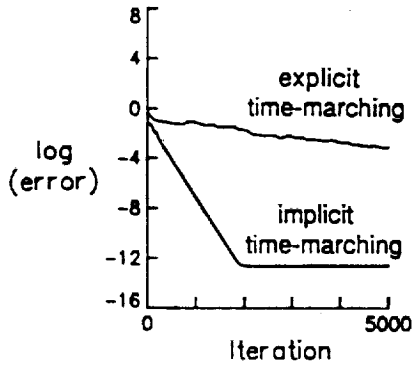

(a) convergence histories.

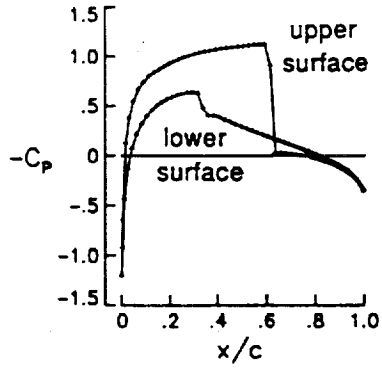

(b) steady pressure distribution.

Fig. 7 Comparisons of steady-state results for the NACA 0012 airfoil at M_∞ = 0.8 and α_o = 1.25° computed using the upwind-type Euler flow solver with flux-vector splitting.

are shown in Fig. 5. For this case the freestream Mach number was M_∞ = 0.8 and the angle of attack was α_o = 0°. Comparisons are given among results obtained using the so-called pulse transfer-function analysis, the harmonic analysis, and a harmonic analysis performed using a structured grid Navier-Stokes code (CFL3D) run in an Euler mode. The three sets of results agree well with one another, for both plunge and pitch motions, thus verifying the accuracy of the unstructured grid method.

Aeroelastic results were also obtained for the NACA 0012 airfoil with two degrees-of-freedom (pitch and plunge) at M_∞= 0.8 and α_o = 0°.[11] Comparisons of second mode generalized displacements (q_2) are shown in Fig. 6 for three values of nondimensional dynamic pressure ($\bar{Q}$) that bracket the flutter point. The generalized displacements agree well with the structured grid (CFL3D) solution which verifies the unstructured grid methodology for aeroelastic analysis. The flutter speed for this case, determined by interpolation of the dominant damping of these generalized displacements, also agrees to within 2% of the CFL3D value.

To test the more-recently-developed upwind-type Euler flow solver, steady flow results were obtained for the NACA 0012 airfoil at $M_\infty = 0.8$ and $\alpha_0 = 1.25°$, using both implicit and explicit time-marching.[15] The explicit time-marching results were obtained using a CFL number of 2.5 and the implicit time-marching results were obtained using a CFL number of 100,000. A comparison of the convergence histories is shown in Fig. 7(a) and the resulting steady pressure distribution is shown in Fig. 7(b). The "error" in the solution was taken to be the L_2–norm of the density residual. As shown, the explicit solution is very slow to converge whereas the implicit solution is converged to four orders of magnitude in only approximately 500 steps. Also, the pressure distributions indicate that there is only one grid point within the shock structure, on either the upper or lower surface of the airfoil, due to the sharp shock capturing ability of the flux splitting. Converged steady solutions are thus obtained with the implicit algorithm with an order of magnitude less CPU time than the explicit algorithm, and the shock waves are more sharply captured with the flux-split spatial discretization than the central-difference-type discretization. These improvements in accuracy and efficiency are also realized for unsteady applications.

Conical Euler Results

Calculations were performed using the conical Euler version of the central-difference-type flow solver to investigate unsteady vortex-dominated flows about highly-swept delta wings.[14] This code includes the additional analysis of the free-to-roll case by the inclusion of the rigid-body equation of motion for simultaneous time integration with the governing flow equations. Results were obtained for a 75° swept delta wing at a freestream Mach number of 1.2 and an angle of attack of 30°. A partial view of the grid which was used is shown in Fig. 8. The grid, which has a total of 4226 nodes and 8299 elements, indicates that the wing has thickness and sharp leading edges.

Figure 9 shows the free-to-roll response of the wing which was initiated by using an initial angular velocity. In this calculation, for simplicity, the mesh was moved to conform to the instantaneous position of the wing by rotating rigidly according to the wing roll angle, rather than by using the deforming mesh algorithm. The results indicate that initially the oscillatory response diverges for small values of roll angle. As the angle increases to around 35°, the rate of divergence decreases due to stabilizing aerodynamics, and finally, the response reaches a maximum amplitude of motion at $\phi = 38°$ corresponding to a limit cycle. These results are similar in nature to those obtained by Arena and Nelson[22] in a low-speed experimental investigation of wing rock. The wing-rock time history from Ref. 22, shown in Fig. 10, was obtained for an 80° swept delta wing at 30° angle of attack. Although the case considered in Fig. 9 is different from that of Ref. 22 (the data from Ref. 22 are for low speed flows whereas the conical Euler code is limited to supersonic freestream applications), the similarity between the two sets of results in Figs. 9 and 10 is noteworthy and gives credibility to the present calculations.

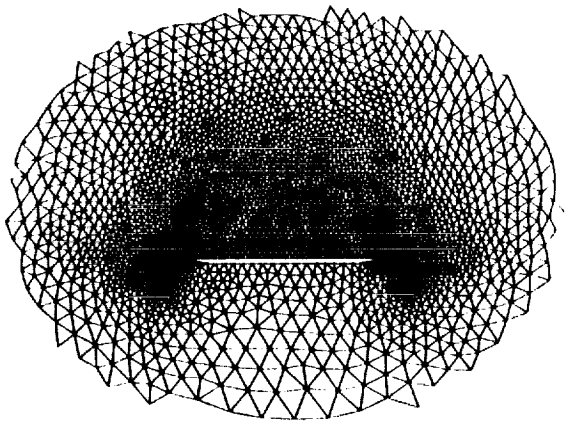

Fig. 8 Partial view of unstructured grid about a 75° swept delta wing.

Three-Dimensional Euler Results

Unsteady flow results were obtained for a supersonic fighter configuration that was oscillating in a complete-vehicle bending mode to demonstrate a three-dimensional application of the central-difference-type Euler solver.[12] The results were obtained using a grid which has 13,832 nodes and 70,125 tetrahedra. The surface triangulation of the aircraft is shown in Fig. 11(a) and the bending mode shape (exaggerated by a factor of five) is shown in Fig. 11(b). Instantaneous pressure distributions on the surface of the vehicle at the maximum (bend-up) and minimum (bend-down) amplitudes of oscillation are shown in Fig. 12. For this case the freestream Mach number was 2.0, the reduced frequency (based on wing tip semi-chord) was 0.1, and two angles of attack of 0 and 12 degrees were considered. The results of Fig. 12 show the effects of angle of attack on unsteady pressures, and clearly demonstrate that the unstructured grid methodology can treat complex aircraft configurations undergoing structural deformation.

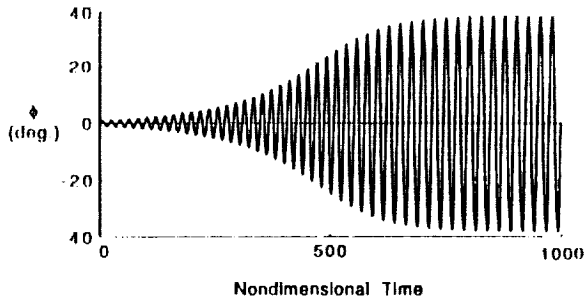

Fig. 9 Free-to-roll time history for a 75° swept delta wing at $M_\infty = 1.2$ and $\alpha = 30°$.

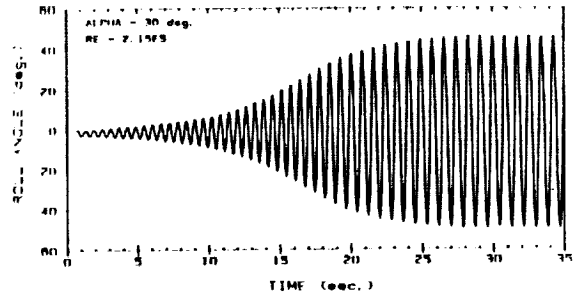

Fig. 10 Wing-rock time history for an 80° swept delta wing at 30° angle of attack (Ref. 22, reprinted with permission from Professor Robert C. Nelson, Notre Dame University).

To test the more-recently-developed upwind-type Euler flow solver, calculations were performed for the ONERA-M6 wing.[16] The M6 wing has a leading edge sweep angle of 30°, an aspect ratio of 3.8, and a taper ratio of 0.562. The airfoil section of the wing is the ONERA "D" airfoil which is a 10% maximum thickness-to-chord ratio conventional section. The results were obtained using a grid which has 42,410 nodes and 231,507 tetrahedra. Results were obtained for the M6 wing at a freestream Mach number of 0.84 and 3.06° angle of attack. These conditions were chosen for comparison with the experimental pressure data of Ref. 23 as shown in Fig. 13. The results indicate that there is a weak supersonic-to-supersonic

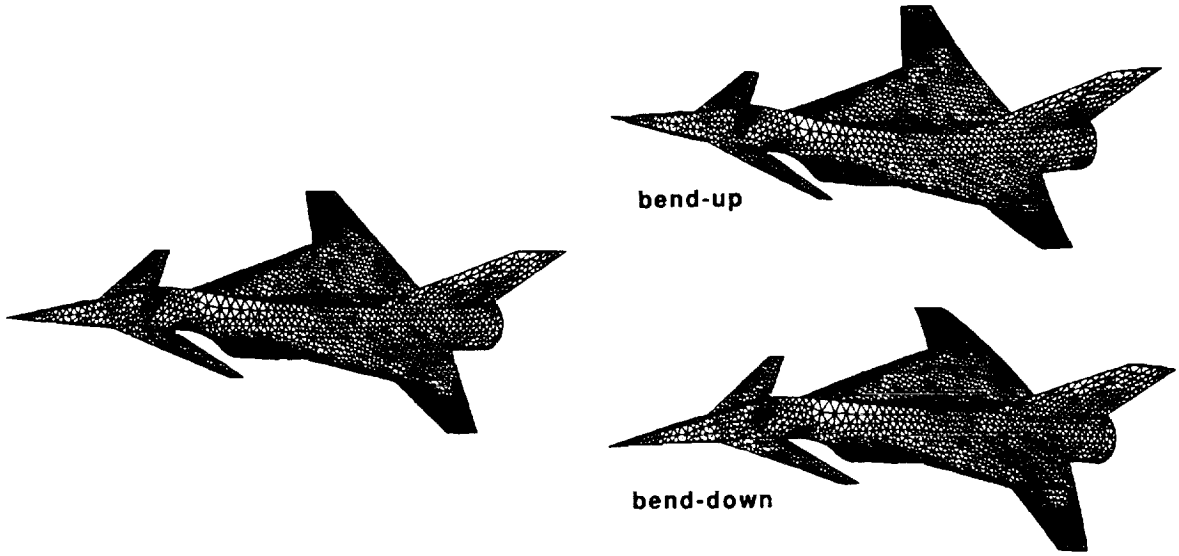

(a) original surface grid.

(b) assumed bending mode.

Fig. 11 Surface grid for the Langley supersonic fighter configuration.

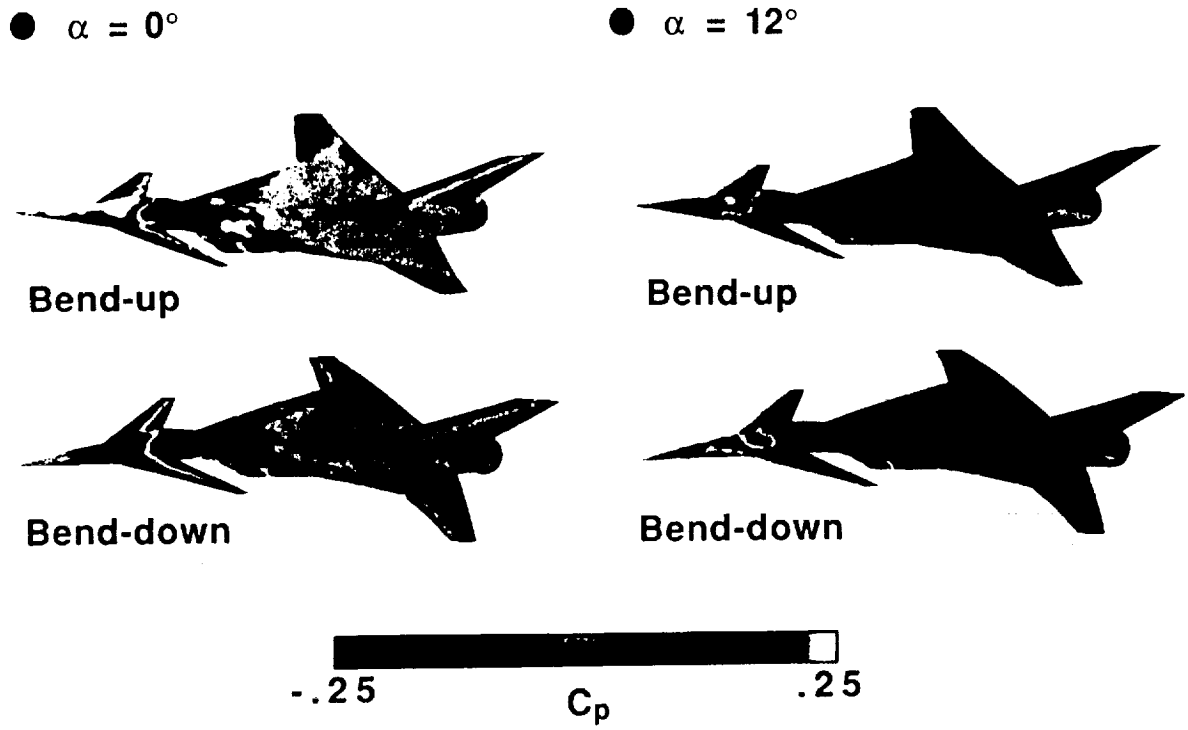

Fig. 12 Effects of angle of attack on the instantaneous pressure coefficient contours on the Langley fighter configuration at the maximum (bend-up) and minimum (bend-down) amplitudes of deformation computed using the central-difference-type Euler flow solver at M_∞ = 2.0 and k = 0.1.

shock wave in the inboard region, forward toward the leading-edge. The primary, supersonic-to-subsonic shock which occurs in the midchord region coalesces with the first shock in the outboard direction toward the wing tip. Near the tip, the two shocks merge to form a single, strong, supersonic-to-subsonic shock wave. The Euler results are in fairly good agreement with the experimental pressure data, especially in predicting the strength and location of the shock waves, which tends to verify the upwind-type algorithm. The shocks are sharply captured with only one grid point within the shock structure, due to the flux splitting.

Spatial Adaption Results

To demonstrate the spatial adaption procedures, results are obtained for the NACA 0012 airfoil pitching harmonically about the quarter chord.[19] The freestream Mach number was 0.755 and the mean angle of attack was 0.016°. The pitching amplitude was 2.51° and the reduced frequency (based on semi-chord) was 0.0814. Figure 14 shows the instantaneous adapted meshes and Fig. 15 shows the corresponding instantaneous density contour lines ($\Delta\rho$ = 0.02). The instantaneous meshes and density contour lines during the third cycle of motion were plotted at eight points in time. In each plot, the instantaneous pitch angle $\alpha(\tau)$ and the instantaneous angular position $k\tau$ in the cycle are noted. The instantaneous meshes (Fig. 14) clearly indicate the enrichment in regions near the shock waves and near the stagnation points. They also show coarsened regions where previously enriched regions have relatively small flow gradients. The density contours during the cycle (Fig. 15) demonstrate the ability of the spatial adaption procedures to produce sharp transient shock waves.

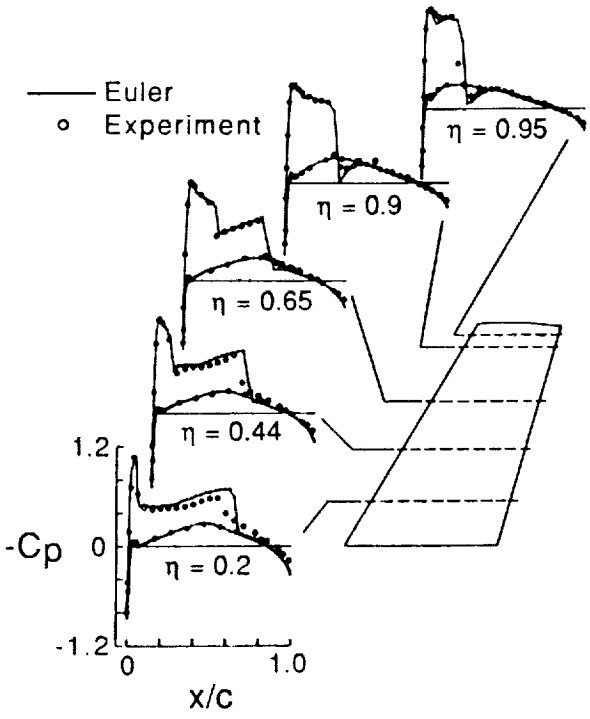

Fig. 13 Comparisons of steady pressure distributions for the ONERA M6 wing computed using the upwind-type Euler flow solver with flux-vector splitting at M_∞ = 0.84 and α_a = 3.06°.

Temporal Adaption Results

To demonstrate the efficiency of temporal adaption over global time-stepping for unsteady problems, results were obtained for the same NACA 0012 pitching airfoil case of the previous section.[18] Figure 16 shows calculated results obtained using temporal adaption and global time-stepping as well as comparisons with the experimental pressure data of Ref. 24. In each pressure plot the instantaneous pitch angle $\alpha(\tau)$ and the angular position in the cycle $k\tau$ are noted. During the first part of the cycle there is a shock wave on the upper surface of the airfoil, and the flow over the lower surface is predominately subcritical. During the latter part of the cycle the flow about the upper surface is subcritical, and a shock forms along the lower surface. The pressure distributions indicate that the shock position oscillates over approximately 25% of the chord along each surface, and in general, that the two sets of calculated results compare well with each other. This good agreement verifies the time-accuracy of the solution computed using temporal adaption, which was obtained at one-fourth of the CPU time that the global time-stepping solution required. Both sets of calculated results also agree well with the experimental data.

Concluding Remarks

The current status of unstructured-grid methods development in the Unsteady Aerodynamics Branch at NASA Langley Research Center was described. These methods are being developed for unsteady aerodynamic and aeroelastic analyses. The paper highlighted the flow solvers that have been developed for the solution of the unsteady Euler equations and gave selected results which demonstrated various features of the capability. The results demonstrated two- and three-dimensional applications for both steady and unsteady flows. Comparisons of two-dimensional steady and unsteady results were made with solutions obtained using a structured grid code and with experimental data to determine the accuracy of the two dimensional flow solvers. Comparisons of three-dimensional steady results were also made with experimental data to determine the accuracy of the three-dimensional flow solver. These comparisons showed good agreement which thus verifies the accuracy of the unstructured grid methods.

Acknowledgements

The authors acknowledge Ken Morgan of the University College of Swansea, UK, and Jaime Peraire of the Imperial College of Science, Technology, and Medicine, London, UK, for providing meshes for the F/A-18 and Langley fighters, and for providing the two-dimensional grid generation program that was used to generate meshes for the delta wing cross section and the NACA 0012 airfoil. The authors also acknowledge Rainald Lohner, George Washington University, Washington, D. C., and Paresh Parikh, ViGYAN Research Associates, Hampton, Virginia, for providing meshes for the Pathfinder I configuration and M6 wing, and for providing the two-dimensional grid generation program that was used to generate meshes for the NACA 0012 airfoil.

References

1. Jameson, A.: "Successes and Challenges in Computational Aerodynamics," AIAA Paper No. 87-1184, January 1987.

2. Edwards, J. W.; and Thomas, J. L.: "Computational Methods for Unsteady Transonic Flows," AIAA Paper No. 87–0107, January 1987.

3. Jameson, A.; and Mavriplis, D. J.: "Finite Volume Solution of the Two-Dimensional Euler Equations on a Regular Triangular Mesh," AIAA Journal, vol. 24, April 1986, pp. 611–618.

4. Mavriplis, D. J.: "Multigrid Solution of the Two-Dimensional Euler Equations on Unstructured Triangular Meshes," AIAA Journal, vol. 26, July 1988, pp. 824–831.

5. Jameson, A.; Baker, T. J.; and Weatherill, N. P.: "Calculation of Inviscid Transonic Flow Over a Complete Aircraft," AIAA Paper No. 86–0103, January 1986.

6. Morgan, K.; and Peraire, J.: "Finite Element Methods for Compressible Flow," Von Karman Institute for Fluid Dynamics Lecture Series 1987–04, Computational Fluid Dynamics, March 2–6, 1987.

7. Lohner, R.: "Finite Elements in CFD: What Lies Ahead," International Journal of Numerical Methods in Engineering, vol. 24, 1987, pp. 1741–1756.

8. Morgan, K.; Peraire, J.; Thareja, R. R.; and Stewart, J. R.: "An Adaptive Finite Element Scheme for the Euler and

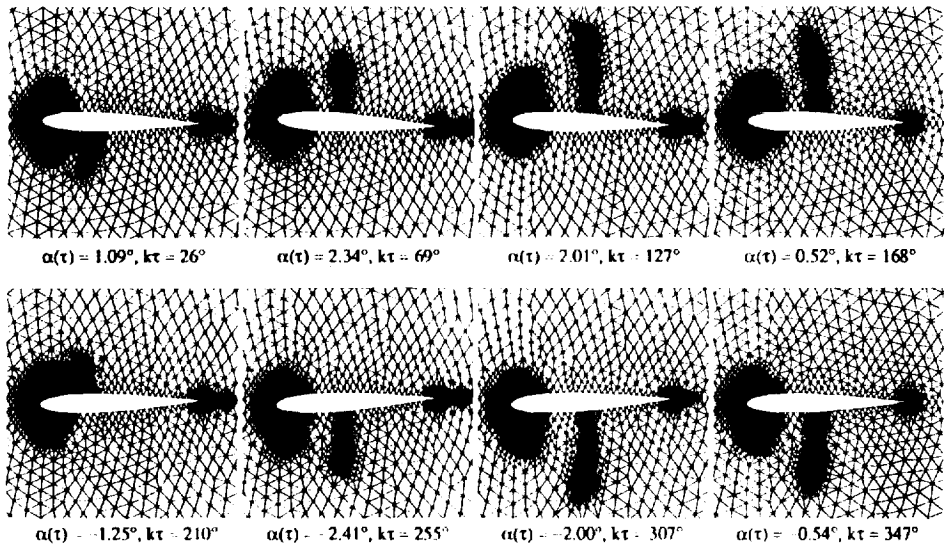

Fig. 14 Instantaneous meshes produced by the spatial adaption procedure for the NACA 0012 airfoil pitching harmonically at $M_\infty = 0.755$, $\alpha_0 = 0.016°$, $\alpha_1 = 2.51°$, and $k = 0.0814$.

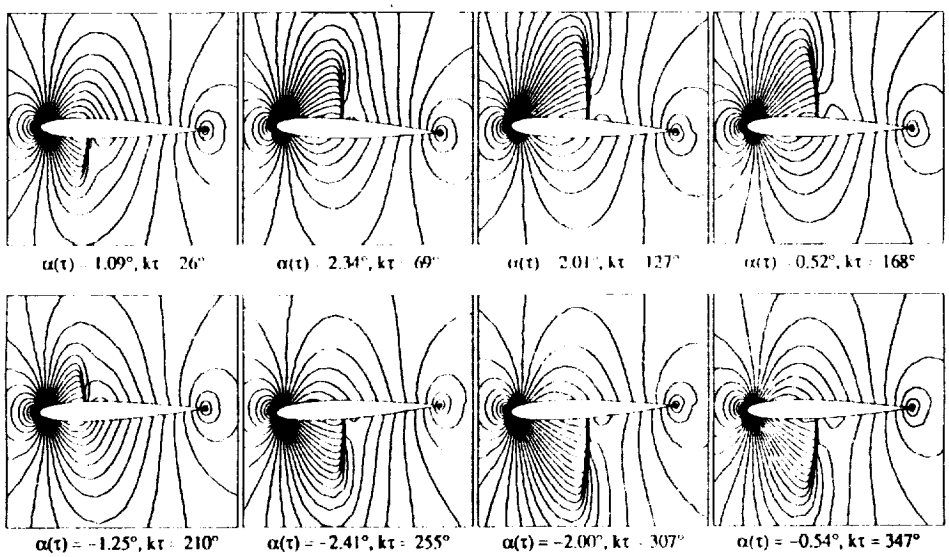

Fig. 15 Instantaneous contour lines ($\Delta\rho = 0.02$) from the spatially adapted solution for the NACA 0012 airfoil pitching harmonically at $M_\infty = 0.755$, $\alpha_0 = 0.016°$, $\alpha_1 = 2.51°$, and $k = 0.0814$.

Navier-Stokes Equations," AIAA Paper No. 87-1172, 1987.

9. Peraire, J.; Peiro, J.; Formaggia, L.; and Morgan, K.: "Finite Element Euler Computations in Three Dimensions," AIAA Paper No. 88-0032, January 1988.

10. Batina, J. T.: "Unsteady Euler Airfoil Solutions Using Unstructured Dynamic Meshes," AIAA Paper No. 89-0115, January 1989.

11. Rausch, R. D.; Batina, J. T.; and Yang, H. T. Y.: "Euler Flutter Analysis of Airfoils Using Unstructured Dynamic Meshes," AIAA Paper No. 89-1384, April 1989.

12. Batina, J. T.: "Unsteady Euler Algorithm with Unstructured Dynamic Mesh for Complex-Aircraft Aeroelastic Analysis," AIAA Paper No. 89-1189, April 1989.

13. Batina, J. T.: "Vortex-Dominated Conical-Flow Computations Using Unstructured Adaptively-Refined Meshes," AIAA Paper No. 89-1816, June 1989.

14. Lee, E. M., and Batina, J. T.: "Conical Euler Solution for a Highly-Swept Delta Wing Undergoing Wing-Rock Motion," NASA TM 102609, March 1990.

15. Batina, J. T.: "Implicit Flux-Split Euler Schemes for Unsteady Aerodynamic Analysis Involving Unstructured Dynamic Meshes," AIAA Paper No. 90-0936, April 1990.

16. Batina, J. T.: "Accuracy of an Unstructured-Grid Upwind-Euler Algorithm for the ONERA M6 Wing," presented at the Accuracy of Unstructured Grid Techniques Workshop, NASA Langley Research Center, Hampton, Virginia, January 16-17, 1990.

17. Batina, J. T.: "Three-Dimensional Flux-Split Euler Schemes Involving Unstructured Dynamic Meshes," AIAA Paper No. 90-1649, June 1990.

18. Kleb, W. L.; Batina, J. T.; and Williams, M. H.: "Temporal Adaptive Euler/Navier-Stokes Algorithm for Unsteady Aerodynamic Analysis of Airfoils Using Unstructured Dynamic Meshes," AIAA Paper No. 90-1650, June 1990.

19. Rausch, R. D.; Batina, J. T.; and Yang, H. T. Y.: "Spatial Adaption Procedures on Unstructured Meshes for Accurate Unsteady Aerodynamic Flow Computation," AIAA Paper No. 91-1106, April 1991.

20. Van Leer, B.: "Flux-Vector Splitting for the Euler Equations," Lecture Notes in Physics, vol. 170, 1982, pp. 507-512.

21. Roe, P. L.: "Approximate Riemann Solvers, Parameter Vectors, and Difference Schemes," Journal of Computational Physics, vol. 43, 1981, pp. 357-372.

22. Arena, A. S.; and Nelson, R. C.: "The Effect of Asymmetric Vortex Wake Characteristics on a Slender Delta Wing Undergoing Wing Rock Motion," AIAA Paper No. 89-3348, August 1989.

23. Schmitt, V.; and Charpin, F.: "Pressure Distribution on the ONERA M6 Wing at Transonic Mach Numbers," Appendix B1 in AGARD-AR-138, Experimental Data Base for Computer Program Assessment, May 1979.

24. Landon, R. H.: "NACA 0012. Oscillating and Transient Pitching," Data Set 3 in AGARD-R-702, Compendium of Unsteady Aerodynamic Measurements, August 1982.

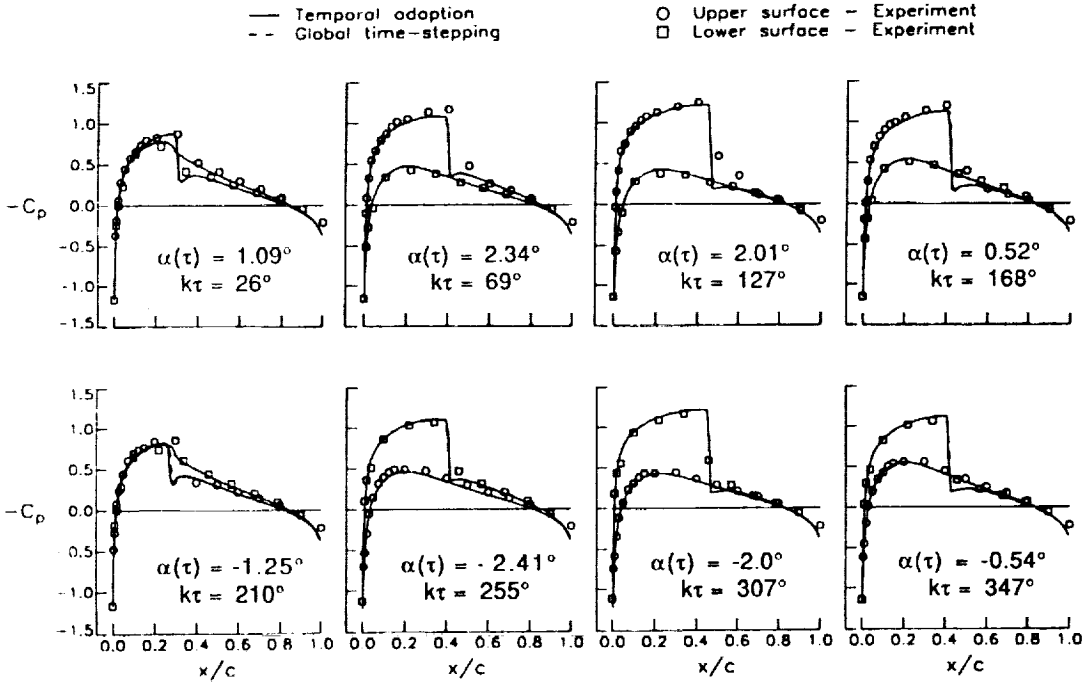

Fig. 16 Comparison of instantaneous pressure distributions for the NACA 0012 airfoil pitching harmonically at $M_\infty = 0.755$, $\alpha_0 = 0.016°$, $\alpha_1 = 2.51°$, and k = 0.0814 computed using the upwind-type Euler flow solver with flux-vector splitting.

Report Documentation Page

1. Report No.	2. Government Accession No.	3. Recipient's Catalog No.
NASA TM 104143		

4. Title and Subtitle
Unstructured-Grid Methods Development for Unsteady Aerodynamic and Aeroelastic Analyses

5. Report Date
September 1991

6. Performing Organization Code

7. Author(s)
John T. Batina, Elizabeth M. Lee, William L. Kleb, and Russ D. Rausch

8. Performing Organization Report No.

10. Work Unit No.
509-10-02-03

9. Performing Organization Name and Address
NASA Langley Research Center
Hampton, Virginia 23665-5225

11. Contract or Grant No.

13. Type of Report and Period Covered
Technical Memorandum

12. Sponsoring Agency Name and Address
National Aeronautics and Space Administration
Washington, DC 20546-0001

14. Sponsoring Agency Code

15. Supplementary Notes
This paper was presented at the AGARD Structures and Materials Panel Specialists Meeting in San Diego, California, on October 6-11, 1991.

16. Abstract

The current status of unstructured-grid methods development in the Unsteady Aerodynamics Branch at NASA Langley Research Center is described. These methods are being developed for unsteady aerodynamic and aeroelastic analyses. The paper first highlights the flow solvers that have been developed for the solution of the unsteady Euler equations and then gives selected results which demonstrate various features of the capability. The results demonstrate two- and three-dimensional applications for both steady and unsteady flows. Comparisons are also made with solutions obtained using a structured grid code and with experimental data to determine the accuracy of the unstructured grid methodology. These comparisons show good agreement which thus verifies the accuracy.

17. Key Words (Suggested by Author(s))	18. Distribution Statement
Unsteady aerodynamics Aeroelasticity Computational fluid dynamics	Unclassified - Unlimited Subject Category 02

19. Security Classif. (of this report)	20. Security Classif. (of this page)	21. No. of pages	22. Price
Unclassified	Unclassified	11	A03

NASA FORM 1626 OCT 86